AGU PUBLICATIONS

Geophysical Research Letters

RESEARCH LETTER
10.1002/2017GL075765

Key Points:
- We quantitatively determine how and how fast magnetopause reconnection spreads in local time and test the observations with theories
- The spreading speed is a few hundred m/s at the cusp ionosphere, and a few ten km/s at the magnetopause
- The spreading speed is more consistent with the magnetopause current carrier speed than the Alfvén speed under strong guide field

Supporting Information:
- Supporting Information S1

Correspondence to:
Y. Zou,
yingzou@bu.edu

Citation:
Zou, Y., Walsh, B. M., Nishimura, Y., Angelopoulos, V., Ruohoniemi, J. M., McWilliams, K. A., & Nishitani, N. (2018). Spreading speed of magnetopause reconnection X-lines using ground-satellite coordination. *Geophysical Research Letters*, *45*, 80–89. https://doi.org/10.1002/2017GL075765

Received 22 SEP 2017
Accepted 17 DEC 2017
Accepted article online 22 DEC 2017
Published online 11 JAN 2018

Spreading Speed of Magnetopause Reconnection X-Lines Using Ground-Satellite Coordination

Ying Zou[1,2], Brian M. Walsh[3], Yukitoshi Nishimura[4,5], Vassilis Angelopoulos[6], J. Michael Ruohoniemi[7], Kathryn A. McWilliams[8], and Nozomu Nishitani[9]

[1]Department of Astronomy and Center for Space Physics, Boston University, Boston, MA, USA, [2]Cooperative Programs for the Advancement of Earth System Science, University Corporation for Atmospheric Research, Boulder, CO, USA, [3]Department of Mechanical Engineering and Center for Space Physics, Boston University, Boston, MA, USA, [4]Department of Electrical and Computer Engineering and Center for Space Sciences, Boston University, Boston, MA, USA, [5]Department of Atmospheric and Oceanic Sciences, University of California, Los Angeles, CA, USA, [6]Department of Earth, Planetary and Space Sciences, University of California, Los Angeles, CA, USA, [7]The Bradley Department of Electrical and Computer Engineering, Virginia Tech, Blacksburg, VA, USA, [8]Institute of Space and Atmospheric Studies, University of Saskatchewan, Saskatoon, Saskatchewan, Canada, [9]Center for International Collaborative Research, Institute for Space-Earth Environmental Research, Nagoya University, Nagoya, Japan

Abstract Conceptual and numerical models predict that magnetic reconnection starts at a localized region and then spreads out of the reconnection plane. At the Earth's magnetopause this spreading would occur primarily in local time along the boundary. Different simulations have found the spreading to occur at different speeds such as the Alfvén speed and speed of the current carriers. We use conjugate Time History of Events and Macroscale Interactions during Substorms (THEMIS) spacecraft and Super Dual Auroral Radar Network (SuperDARN) radar measurements to observationally determine the X-line spreading speed at the magnetopause. THEMIS probes the reconnection parameters locally, and SuperDARN tracks the reconnection development remotely. Spreading speeds under different magnetopause boundary conditions are obtained and compared with model predictions. We find that while spreading under weak guide field could be explained by either the current carriers or the Alfvén waves, spreading under strong guide field is consistent only with the current carriers.

1. Introduction

Although magnetic reconnection is a three-dimensional phenomenon with a finite extent out of the reconnection plane, knowledge of how reconnection progresses out of the plane remains primitive. At the subsolar point of the magnetopause, the reconnection plane roughly corresponds to the GSM *X-Z* plane. Numerical simulations agree that reconnection begins with a short X-line, and the X-line spreads over time (Huba & Rudakov, 2002; Jain et al., 2013; Lapenta et al., 2006; Nakamura et al., 2012; Shay et al., 2003). How and how quickly the X-line spreads is less defined. Spreading is thought to occur in the direction of the current carriers of the reconnecting current sheet, either electrons or ions. It is suggested to occur at a speed associated with the current carrier speed (Lapenta et al., 2006; Nakamura et al., 2012; Shay et al., 2003). The mechanism is attributed to the decoupling of electrons and ions in the current sheet, where electrons carry magnetic field lines toward one direction, and the plasma is depleted toward the other direction (that of the ion motion) (Lapenta et al., 2006; Nakamura et al., 2012; Shay et al., 2003). This results in a thinning of the current sheet over an increasingly extended region, which effectively broadens the reconnection region.

The X-line spreading geometry changes with the introduction of a guide field. Shepherd and Cassak (2012) found that under strong guide field spreading occurs bidirectionally and at a speed consistent with the Alfvén speed based on the guide field. They proposed that rather than being driven solely by the current carriers, spreading is also driven by the Alfvén waves propagating along the guide field and that spreading is governed by the faster of the two mechanisms (current carriers or Alfvén waves) in each direction.

Experimental studies have attempted to observe X-line spreading and compare with the model predictions. In laboratory experiments, the X-line was found to spread with and without guide fields. Although it spread in a direction consistent with the predictions, the speed from these experiments was a fraction of the electron drift speed under no guide field (Dorfman et al., 2013, 2014) and equaled twice the Alfvén speed under strong guide field conditions (Katz et al., 2010). Reconnection can also be remotely imaged at solar flares. Flare

ribbons are observed to spread along the magnetic polarity inversion line unidirectionally or bidirectionally (Cheng, Kerr, & Qiu, 2012; Fletcher, Pollock, & Potts, 2004; Lee & Gary, 2008; Liu et al., 2010; Qiu, 2009; Qiu et al., 2010, 2017). Qiu et al. (2017) found that although flare ribbons may tend to spread bidirectionally under a strong guide field, consistent with theory, the speed is an order of magnitude smaller than the Alfvén speed. The speed of the current carriers cannot be obtained from the flare images, which limits the comparison. The spreading speed is a key parameter to compare with simulations, as bidirectional spreading can result from both propagation of the Alfvén waves and motion of the current carriers when ions and electrons both carry the current.

The Earth's magnetosphere provides an advantageous observational environment for determining the properties and physical mechanism of X-line spreading. This is because the magnetic field and plasma conditions can be probed in situ at the Earth, rather than remotely inferring these parameters at the Sun. Although spacecraft can only monitor reconnection at one or several points (e.g., Alexandrova et al., 2015; Walsh, Komar, & Pfau-Kempf, 2017; Zhou et al., 2017), ground-based measurements can provide a wider field of view of the reconnection rate and extent over time. When reconnection is active at the dayside magnetopause, the electric potential along the reconnection X-line can map along field lines to the ionosphere and drive ionospheric plasma flow across the open-closed field line boundary (e.g., Baker, Rodger, & Lu, 1997; Blanchard et al., 2001; Chisham et al., 2004, 2008; de la Beaujardière et al., 1991; Hubert et al., 2006; Pinnock et al., 1999, 2003; Vasyliunas, 1984). As the newly reconnected flux tubes are carried antisunward, ionospheric plasma at their footprints moves poleward forming a channel of fast flow in the ionosphere (Southwood, 1985). The channel location reflects the X-line location and the channel width reflects the X-line extent (e.g., Goertz et al., 1985; Lee et al., 2016; McWilliams, Yeoman, Sigwarth, et al., 2001; Milan et al., 2000, 2016; Pinnock et al., 1993; Provan, Yeoman, & Milan, 1998; Wild et al., 2001, 2003). This width can remain localized for tens of minutes, well after the flow channel has already propagated deep inside the polar cap (Nishimura et al., 2014; Zou et al., 2015, 2016) (although the width may expand wider than it is at the origin (McWilliams, Yeoman, & Cowley, 2001)).

We use conjugate dayside observations by Time History of Events and Macroscale Interactions during Substorms (THEMIS) (Angelopoulos, 2008) and Super Dual Auroral Radar Network (SuperDARN) (Greenwald et al., 1995), where THEMIS probes the occurrence of magnetopause reconnection and in situ magnetic field and plasma conditions, and SuperDARN measures the width of the related ionospheric flow channels as a function of time. We focus on periods when the interplanetary magnetic field (IMF) from OMNI data strongly rotates from north to south and we manually inspected whether an enhanced poleward directed flow channel formed near the dayside cusp from a quiet background. The satellite should cross the magnetopause within ~10 min of the onset of the flow channel and at a longitude conjugate to the flow channel. Five events have been identified in year 2014–2015, and we present two events that had the best coverage of the azimuthal extent of the flow channel. One event occurred on 23 May 2014, when the magnetopause current carrier speed was slightly larger than the Alfvén speed along the guide field. The other event occurred on 7 February 2014, when the current carrier speed was much smaller than the Alfvén speed. We refer to these two events as weak and strong guide field magnetopause conditions (Shepherd & Cassak, 2012).

2. Observations

2.1. X-Line Spreading Under a Weak Guide Field

2.1.1. Observation of X-Line Spreading: Ground-Based Measurements

On 23 May 2014, the IMF upstream of the Earth's magnetosphere had a strong rotation from positive to negative B_z (Figure 1g). Radar flow measurements are shown in altitude-adjusted corrected geomagnetic coordinates in Figures 1a–1f. The color tiles show line-of-sight (LOS) speeds, and the arrows show merged 2 d velocity vectors that are computed from overlapping LOS velocities. Enhanced (red) and poleward directed flows are the feature of interest. Convection was initially dominated by a clockwise vortex (Figure 1a), which may be a reversed convection cell under a northward IMF (e.g., Burke et al., 1979) or a reconnection-induced flow shear under a strong east-west IMF (McWilliams et al., 2004). This pattern was abruptly replaced by a fast poleward directed flow channel at 1538 UT (Figure 1b), which was ~10 min after the IMF turned south. The lag is due to the IMF propagation from the bow shock to the magnetopause and the signal propagation from the magnetopause to the ionosphere (Wang et al., 2016). The flow channel originated around the open-closed line boundary at ~78° magnetic latitude (MLAT), as estimated from the 150 m/s spectral width

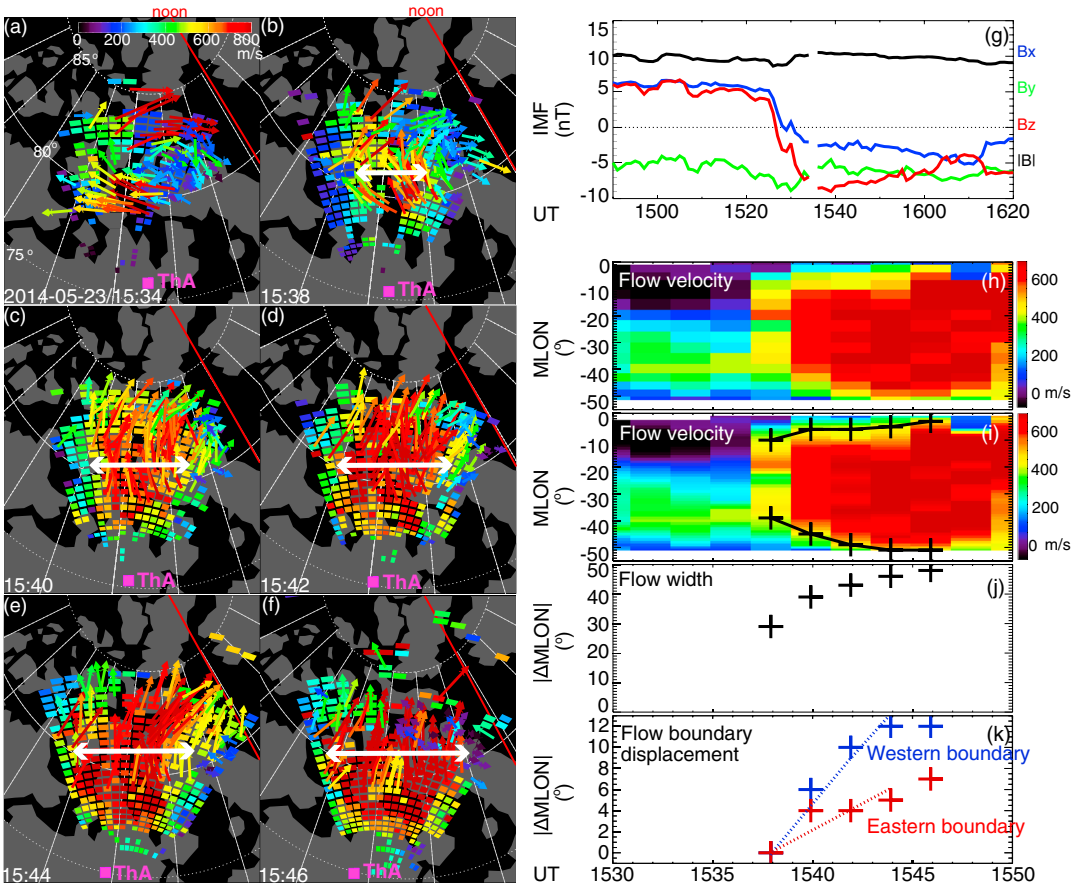

Figure 1. Evolution of an ionospheric flow channel near the dayside cusp on 23 May 2014. (a–f) Snapshots of radar flows measurements (2 min resolution). The color tiles show LOS speed measured by Rankin Inlet radar, and the colors indicate flow speeds moving away from the radar. The arrows show merged vectors measured by Rankin Inlet, Inuvik, and Clyde River radars. The arrow direction indicates flow directions, and the colors and lengths indicate flow speeds. The red and poleward directed arrows are the flow features of our interest, and their width is marked by the white arrows. (g) IMF time-shifted to the bow shock. (h) Ionospheric flow velocity as a function of magnetic longitude and universal time. Each velocity point is averaged over 79–85° MLAT. (i) Similar to Figure 1h but an interpolation is performed over longitude to a resolution of 1°. The plus signs mark the boundaries of the flow channel that delimit the flow channel width. The boundaries are determined with a threshold of 400 m/s. (j) Flow width as a function of time. (k) Displacements of the eastern/western boundary over time from the flow's first appearance. A linear fitting is performed and shown as the blue and red dotted lines.

boundary (Figure S1 in the supporting information) (e.g., Baker et al., 1995, 1997; Chisham & Freeman, 2003). The flow channel was an ionospheric signature of magnetopause reconnection as will be confirmed with the THEMIS measurements below.

The flow channel, once formed, spread azimuthally, its width marked by the white arrows (Figures 1b–1f, width will be defined below). The spreading behavior of the flow channel indicates that the corresponding magnetopause X-line also spread azimuthally.

We now quantitatively track the flow channel width at a fixed latitude just poleward of the open-closed field line boundary (Figure 1h). Each point is an averaged LOS velocity over 79°–85° MLAT. The longitudinal resolution corresponds to radar beam separations (16 beams), and a linear interpolation gives a more continuous velocity distribution (Figure 1i) for determining the flow channel eastern and western boundaries that delimit the extent of the flow channel. The velocity threshold for determining the boundaries is 400 m/s, which is just above the convection speed before the emergence of the flow channel and therefore includes much of the velocity enhancement caused by the southward turning of the IMF. The boundaries are marked by the plus signs connected by the solid lines. They clearly show that the enhanced flow channel suddenly occurred at 1538 UT and spread azimuthally in both directions, which results in an expanding width (Figure 1j). The spreading speeds can be obtained from the displacements of the boundaries over time (Figure 1k). We linearly fit (dotted lines) the displacements using the first 6 min measurements, when the flow channel

boundaries were within the radar field of view (FOV). This gives speeds of 596 ± 244 and 271 ± 190 m/s for the western and eastern boundaries, respectively. The uncertainties are due to the finite radar spatial and temporal resolution.

A careful examination of the western boundary displacement shows that the spreading spread tends to decrease with time. A similar and more prominent trend is seen in the 7 February 2014 event in section 2.2.1. Simulations by Nakamura et al. (2012) suggest a possible two-phase spreading where the spreading was initially fast and then slow. Our speed estimates relate to the fast phase.

We next project such spreading from the ionosphere to the magnetopause using the Tsyganenko magnetic field model (T01) (Tsyganenko, 2002a, 2002b). This is done by field-line mapping a pair of ionospheric locations that are azimuthally separated in the ionosphere (supposedly just equatorward of the open-closed field line boundary) to the equatorial plane. The ratio of the pair separation in the equatorial plane to that in the ionosphere gives a mapping factor. Since the field-line geometry can change considerably around the last closed field lines, we obtain the possible range of the mapping factor by performing mapping repetitively over a range of latitudes equatorward of the open-closed field line boundary (Figure S2). The mapping factor is 46 ± 18. A similar mapping procedure using the T96 model (Tsyganenko, 1995) gives a factor of 44 ± 16; such a small change will not fundamentally alter our estimate of the X-line spreading speed. The X-line therefore spread at a speed of 27.4 ± 15.5 and 12.5 ± 10.0 km/s at its western and eastern ends.

The open-closed field line boundary in T01 was ~3° equatorward of the observations (Figure S2). This should not affect the mapping factor we obtained significantly. In fact, the boundary in T96 was ~2° equatorward of T01, and the mapping factor changes by only $<$10%.

2.1.2. Observation of X-Line Spreading: Space-Based Measurements

When SuperDARN monitored the flow channel in the ionosphere, THEMIS A encountered the magnetopause. The satellite footprint mapped with the T01 model is shown by the THA marker in Figure 1. Figure 2a shows the satellite location in GSM *Y-Z* plane and its relation to magnetic shear angle across the magnetopause. The angle was calculated following Trattner et al. (2007, 2012), with an input IMF taken from a quasi-steady state following the southward turning of the IMF. The most probable location for reconnection to occur is determined by the ridge of maximum magnetic shear (white plus signs) (Trattner et al., 2007, 2012). THEMIS A was located close to the probable reconnection X-line location, and we therefore can trust its measurements for determining reconnection occurrence and for parameterizing the plasma and magnetic field conditions at the X-line.

Figures 2b–2e present the magnetic field, ion energy flux, ion density, and ion velocity measured by THEMIS A when passing through the magnetopause. The magnetic field and ion velocity components are displayed in the LMN boundary normal coordinate system, obtained from the minimum variance analysis (MVA) of the magnetic field (Sonnerup & Cahill, 1967). The satellite encountered the magnetopause at ~15:51:26–15:51:39 UT and detected an accelerated plasma jet reaching ~400 km/s. The jet velocity satisfied the Walen relation (Hudson, 1970; Paschmann et al., 1979), where the observed speed was 70% and the angle was within ~15° of Walen predictions, providing a fluid confirmation of the occurrence of magnetic reconnection (Phan et al., 1996, 2013). In addition to the clear jet, the spacecraft measured a D-shape distribution inside the magnetopause current sheet (Figure 2f), a kinetic signature of reconnection (Cowley, 1982). The measurements confirm that reconnection was active and was the magnetospheric counterpart of the ionospheric flow channel seen by SuperDARN.

2.1.3. Comparison of Observation and Theory

Measurements of the local plasma environment at the current sheet near the X-line enable us to test the theoretically proposed mechanisms of X-line spreading. Here we compare the observed speeds with that of the current carriers and the Alfvén speed studied by Shepherd and Cassak (2012). The speed of current carriers is expressed as

$$V_{\text{current}} = \frac{J}{ne} = \frac{\left(\frac{\Delta B_l}{\mu_o d}\right)}{ne} \tag{1}$$

where B_l is the L component of the magnetic field, i.e., the reconnecting magnetic field, d is the thickness of the current layer (magnetopause in this study), n is the plasma number density, and e is the elementary charge. Here we have assumed the magnetopause to be a planar current sheet. The out-of-plane Alfvén speed is

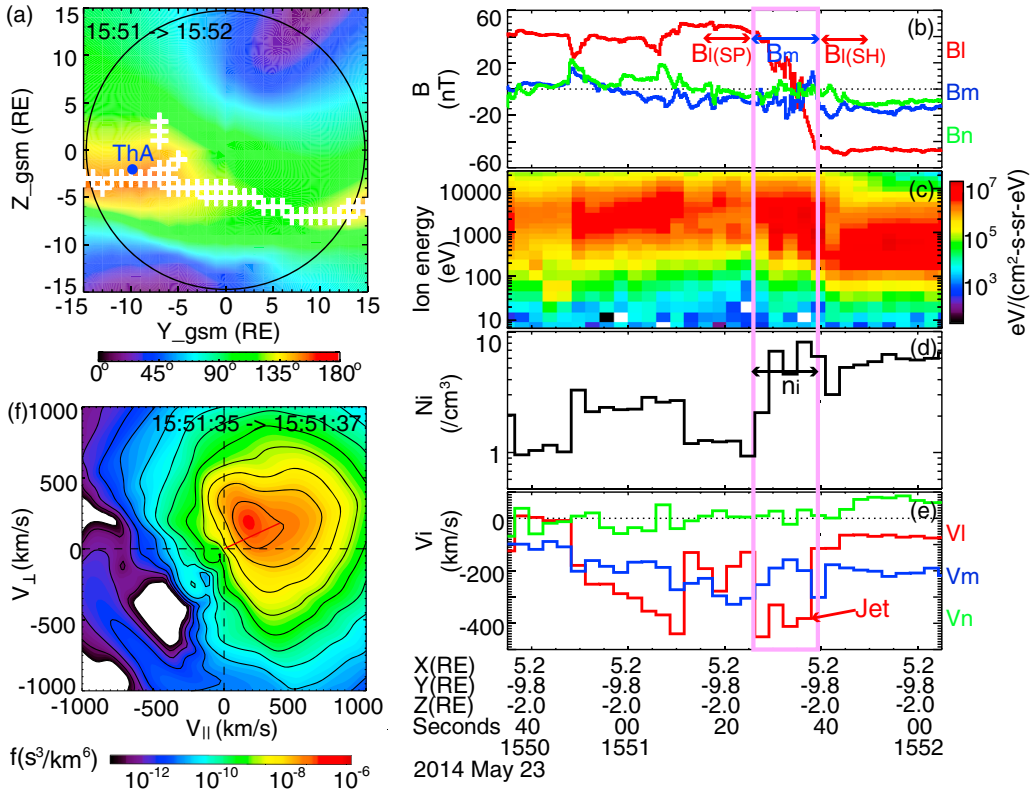

Figure 2. THEMIS A measurements during the ionospheric flow channel shown in Figure 1. (a) The location of the satellite in GSM *Y-Z* plane and the magnetopause shear angle viewed from the Sun. Locations of maximum shear angle are marked by the white plus signs. The black circle represents the size of the magnetopause at the terminator. (b–e) Measured magnetic field (0.25 s resolution), ion energy flux (3 s), ion density (3 s), and ion velocity (3 s). The ion measurements were taken from ground ESA moments. The pink box identifies the magnetopause. $B_{l(SP)}$, $B_{l(SH)}$, B_m, and n_i represent L component of magnetic field in the magnetosphere and magnetosheath, M component at the magnetopause, and ion density at the magnetopause. (f) Ion distribution function on the bulk velocity-magnetic field plane. The small red line indicates the direction and bulk velocity of the distributions.

$$V_{\text{Alfv\'en}} = \frac{B_m}{\sqrt{\mu_o n m_i}} \tag{2}$$

where B_m is the M component of the magnetic field, i.e., the guide field, and m_i is the proton mass. Here we have assumed the ions to comprise protons only. All quantities except the magnetopause thickness can be readily determined from the satellite measurements. We determine ΔB_l as the difference between the B_l components just inside and outside the magnetopause averaged over the 10 s windows, n as the local ion density averaged over the magnetopause, and B_m as the B_m component averaged over the magnetopause (Figure 2b).

The magnetopause thickness used is 940 ± 345 km, which is identified from statistical multispacecraft measurements at the magnetopause (Figure 7 of Berchem & Russell, 1982). Here the uncertainty is the standard deviation of the thickness distribution in their study. The magnetopause thickness measured by a single satellite is subject to spatial-temporal ambiguity (Bauer et al., 2000; Haaland et al., 2004) and can suggest a value different from the multispacecraft measurements by a factor of 2 or more (Bauer et al., 2000). For interested readers, we have estimated the thickness using THEMIS A measurements, where we multiply the deHoffmann-Teller frame velocity of the magnetopause along the boundary normal direction by the time the magnetopause past THEMIS A. The thickness is estimated to be 744 ± 638 km. We do not use this number because of the large uncertainty arising from determining the magnetopause normal direction, but this estimate is roughly consistent with the thickness in Berchem and Russell (1982).

Table 1 lists the values used for equations (1) and (2) and the obtained current carrier speed and out-of-plane Alfvén speed. Except for the thickness, the uncertainties are the 95% confidence interval for the means. The current carrier speed and Alfvén speed were 89.8 ± 77.7 and 60.9 ± 33.4 km/s. As a reminder, the X-line

Table 1
From Top to Bottom: ΔB_l Component Across the Magnetopause, B_m Component at the Magnetopause, Ion Density at the Magnetopause, Magnetopause Thickness Determined by Berchem and Russell (1982), and the Calculated Current Carrier Speed and Out-of-Plane Alfvén Speed

	23 May 2014 event	7 February 2014 event (MP)	7 February 2014 event (LLBL)
ΔB_l (nT)	91.7 ± 2.8	100.9 ± 2.7	128.1 ± 0.7
B_m (nT)	6.5 ± 2.5	50.6 ± 2.0	48.9 ± 0.8
n_i (cm)	5.4 ± 4.2	26.9 ± 2.6	12.1 ± 0.9
D (km)	940 ± 345	940 ± 345	940 ± 345
$V_{current}$ (km/s)	89.8 ± 77.7	19.8 ± 7.5	56.1 ± 21.0
$V_{Alfvén}$ (km/s)	60.9 ± 33.4	212.7 ± 13.2	306.9 ± 12.9
V_{spread} (km/s)	27.4 ± 15.5 (westward)12.5 ± 10.0 (eastward)	28.8 ± 13.1 (eastward)	28.8 ± 13.1 (eastward)

Note. The observed X-line spreading speeds are also shown at the bottom for comparison. For the 7 February 2014 event, the values are also determined across the LLBL, on condition that the LLBL also affects the X-line spreading. The uncertainty has considered the uncertainty of MVA calculation window.

spreading speed was 27.4 ± 15.5 and 12.5 ± 10.0 km/s at its western and eastern ends. The spreading speed is smaller than the Alfvén speed, but the difference is within or comparable to the uncertainties. The total X-line spreading speed is 39.9 ± 25.5 km/s (summing the electron and ion shares of the current). This is again smaller than but within the uncertainty range of the current carrier speeds. This event therefore suggests that the X-line spreading speed could potentially be explained by either the current carriers or the Alfvén waves. The inequality of the spreading speeds in two directions may suggest an agreement with the often asymmetric current carrier motion but can also result from Alfvén wave propagation in a moving plasma.

2.2. X-Line Spreading Under a Strong Guide Field

A second conjunction is presented with magnetopause reconnection occurring under a strong guide field. In this regime, the spreading speed is predicted to be controlled by the out-of-plane Alfvén speed (Shepherd & Cassak, 2012).

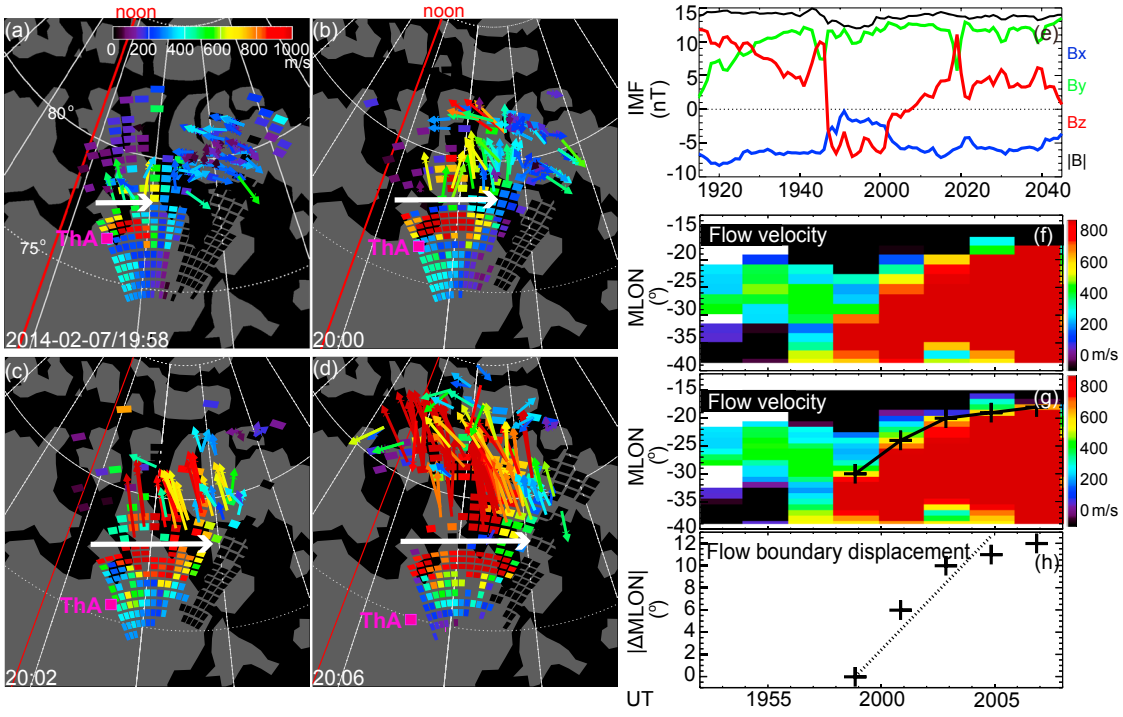

Figure 3. (a–h) Evolution of an ionospheric flow channel on 7 February 2014. Velocity in Figure 3f is averaged over 78–79° MLAT (spectral width boundary at 77–78° MLAT) and the velocity threshold for determining the flow boundary is 500 m/s.

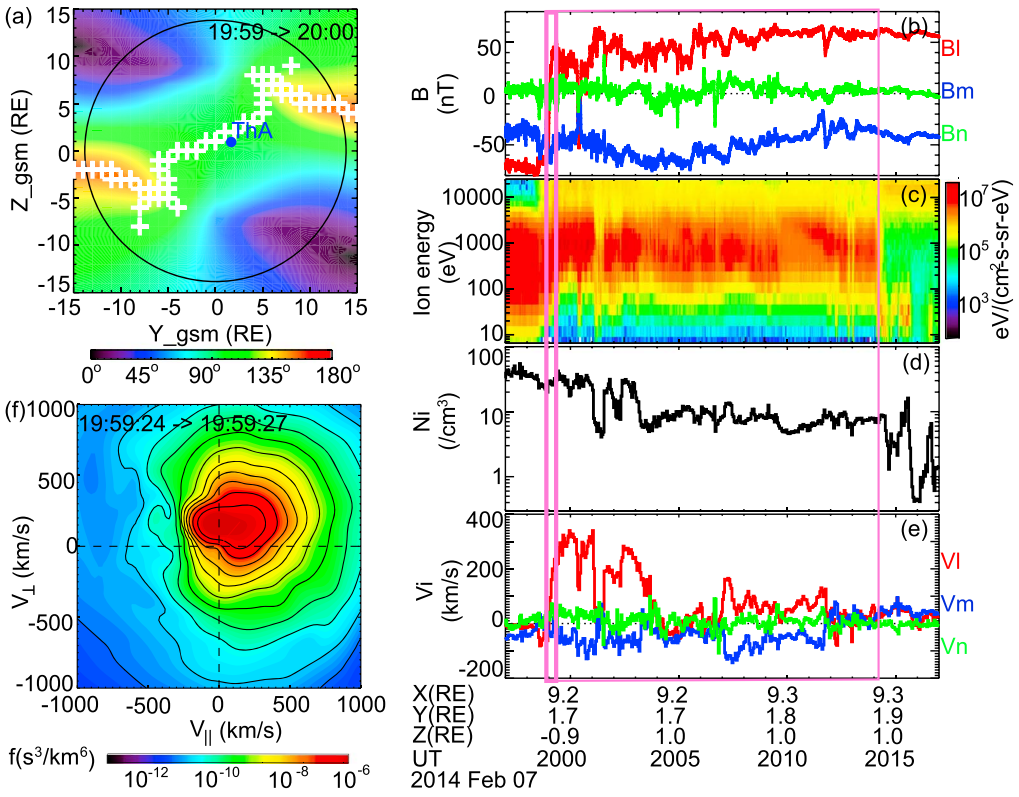

Figure 4. THEMIS A measurements during magnetopause crossing. The magnetopause and low-latitude boundary layer are identified by the thick and thin pink boxes, respectively.

2.2.1. Observation of X-Line Spreading: Ground-Based Measurements

On 7 February 2014, the IMF upstream of the Earth rotated from strong positive B_z to a negative B_z (Figure 3e). This is followed by an enhanced, poleward directed ionospheric flow channel (Figures 3a–3d), which was again an ionospheric signature of magnetopause reconnection. The flow channel spread azimuthally (Figures 3b–3d). We focus on the eastern flow channel boundary since the western boundary quickly spread beyond the radar FOV and because the westernmost radar echoes were contaminated by ground scatter (Blanchard, Sundeen, & Baker, 2009; Chisham & Pinnock, 2002). We linearly fit the motion of the eastern boundary using the first 6 min measurements following section 2.1.1, and obtain a spreading speed of 800 ± 305 m/s in the ionosphere. The mapping ratio for this event is 36 ± 9 under the T01 model (29 ± 8 under T96, difference $<$ 20%). This suggests that the X-line spread duskward at 28.8 ± 13.1 km/s.

2.2.2. Observation of X-Line Spreading: Space-Based Measurements

THEMIS A crossed the magnetopause close to the X-line (Figure 4a). It took ~15 min to traverse the magnetopause and the low-latitude boundary layer (LLBL). The observed plasma jet of 200–300 km/s and the D-shape ion distribution confirm that reconnection was driving the ionospheric flow signature.

2.2.3. Comparison of Observation and Theory

The 7 February 2014 event occurred under a strong guide field, ~50 nT, and the speeds of the Alfvén wave and the current carriers are now of different orders. We determine the guide field strength and ion density by averaging them over the magnetopause (thick pink box in Figures 4b–4e), and over the magnetopause and LLBL as a whole boundary layer (entire pink area), as it is not clear which boundary condition is truly impacting the reconnection. The magnetopause thickness is again adopted from Berchem and Russell (1982) (the single-satellite measurement gives 493 ± 279 km). The results are shown in Table 1. The current carrier speed was 19.8 ± 7.5 and 56.1 ± 21.0 km/s, based on measurements over the magnetopause and the entire boundary layer, respectively. This is similar to the X-line spreading speed (28.8 ± 13.1 km/s). The out-of-plane Alfvén speed, however, was 212.7 ± 13.2 and 306.9 ± 12.9 km/s. The difference of this speed to the spreading speed well exceeds the uncertainties, and therefore, the Alfvén wave is unlikely to be the process governing the spreading.

Therefore, this event provides observational evidence that the X-line spreading speed is related more to the current carrier speed than the out-of-plane Alfvén speed. This observation is different from the prediction by Shepherd and Cassak (2012), where the faster of the two relevant speeds determines the spreading speed. The reason of the difference is unknown, but the idealized configurations of the current layer used in their simulation could be one potential factor (Cassak, personal communication). The current layer used in Shepherd and Cassak (2012) is flat, uniform, and symmetric. The realistic magnetopause is curved, contains possible gradients in density and magnetic field, and has asymmetric plasma environments (density, temperature, and bulk motion) at the two sides of the boundary.

3. Conclusion

We investigated how magnetopause reconnection X-lines spread over local time and what physics drives the spreading using THEMIS-SuperDARN coordination. The X-line under the weak guide field spreads at a speed of 867 ± 434 m/s in the ionosphere and 39.9 ± 25.5 km/s at the magnetopause. The X-line under the strong guide field spreads at 800 ± 305 m/s and 28.8 ± 13.1 km/s. With the THEMIS data, we obtained the in situ speeds of the current carriers and the Alfvén waves and compared with predictions by Shepherd and Cassak (2012). The results suggest that the spreading under the weak guide field could potentially be explained by either the current carriers or the Alfvén waves and that the spreading under the strong guide field condition is consistent only with the current carriers, unless the wave propagates slower than the Alfvén speed due to reasons currently unknown.

This study demonstrates the ability to study X-line spreading at the Earth's magnetopause using ground-space coordination. SuperDARN and THEMIS have been operating continuously for the past 10 years, providing numerous conjunction opportunities. This would permit a thorough study of the characteristics of magnetopause X-line spreading under a variety of solar wind and geomagnetic conditions and solar cycle phases.

Acknowledgments
This research was supported by the NASA Living With a Star Jack Eddy Postdoctoral Fellowship Program, administered by UCAR's Cooperative Programs for the Advancement of Earth System Science (CPAESS), NASA grant NNX15AI62G, NSF grants PLR-1341359 and AGS-1451911, and AFOSR FA9550-15-1-0179 and FA9559-16-1-0364. The THEMIS mission is supported by NASA contract NAS5-02099. SuperDARN is a collection of radars funded by National Science Foundation agencies. SuperDARN Canada is supported by the Canada Foundation for Innovation, the Canadian Space Agency, and the Province of Saskatchewan. Data products of the SuperDARN, THEMIS, and OMNI are available at http://vt.superdarn.org/, http://themis.ssl.berkeley.edu/index.shtml, and GSFC/SPDF OMNIWeb website.

References

Alexandrova, A., Nakamura, R., Semenov, V. S., & Nakamura, T. K. M. (2015). Motion of reconnection region in the Earth's magnetotail. *Geophysical Research Letters*, *42*, 4685–4693. https://doi.org/10.1002/2015GL064421

Angelopoulos, V. (2008). The THEMIS mission. *Space Science Reviews*, *141*(1-4), 5–34. https://doi.org/10.1007/s11214-008-9336-1

Baker, K. B., Dudeney, J. R., Greenwald, R. A., Pinnock, M., Newell, P. T., Rodger, A. S., … Meng, C.-I. (1995). HF radar signatures of the cusp and low-latitude boundary layer. *Journal of Geophysical Research*, *100*, 7671–7695. https://doi.org/10.1029/94JA01481

Baker, K. B., Rodger, A. S., & Lu, G. (1997). HF-radar observations of the dayside magnetic merging rate: A Geospace Environment Modeling boundary layer campaign study. *Journal of Geophysical Research*, *102*, 9603–9617. https://doi.org/10.1029/97JA00288

Bauer, T. M., Dunlop, M. W., Sonnerup, B. U. O., Sckopke, N., Fazakerley, A. N., & Khrabrov, A. V. (2000). Dual spacecraft determinations of magnetopause motion. *Geophysical Research Letters*, *27*, 1835–1838. https://doi.org/10.1029/2000GL000041

Berchem, J., & Russell, C. T. (1982). The thickness of the magnetopause current layer: ISEE 1 and 2 observations. *Journal of Geophysical Research*, *87*, 2108–2114. https://doi.org/10.1029/JA087iA04p02108

Blanchard, G. T., Ellington, C. L., Lyons, L. R., & Rich, F. J. (2001). Incoherent scatter radar identification of the dayside magnetic separatrix and measurement of magnetic reconnection. *Journal of Geophysical Research*, *106*, 8185–8195. https://doi.org/10.1029/2000JA000262

Blanchard, G. T., Sundeen, S., & Baker, K. B. (2009). Probabilistic identification of high-frequency radar backscatter from the ground and ionosphere based on spectral characteristics. *Radio Science*, *44*, RS5012. https://doi.org/10.1029/2009RS004141

Burke, W. J., Kelley, M. C., Sagalyn, R. C., Smiddy, M., & Lai, S. T. (1979). Polar cap electric field structures with a northward interplanetary magnetic field. *Geophysical Research Letters*, *6*, 21–24. https://doi.org/10.1029/GL006i001p00021

Cheng, J. X., Kerr, G., & Qiu, J. (2012). Hard X-ray and ultraviolet observations of the 2005 January 15 two-ribbon flare. *The Astrophysical Journal*, *744*(1), 48. https://doi.org/10.1088/0004-637X/744/1/48

Chisham, G., & Freeman, M. P. (2003). A technique for accurately determining the cusp-region polar cap boundary using SuperDARN HF radar measurements. *Annales Geophysicae*, *21*(4), 983–996. https://doi.org/10.5194/angeo-21-983-2003

Chisham, G., Freeman, M. P., Abel, G. A., Lam, M. M., Pinnock, M., Coleman, I. J., … Villain, J. P. (2008). Remote sensing of the spatial and temporal structure of magnetopause and magnetotail reconnection from the ionosphere. *Reviews of Geophysics*, *46*, RG1004. https://doi.org/10.1029/2007RG000223

Chisham, G., Freeman, M. P., Coleman, I. J., Pinnock, M., Hairston, M. R., Lester, M., & Sofko, G. (2004). Measuring the dayside reconnection rate during an interval of due northward interplanetary magnetic field. *Annales Geophysicae*, *22*, 4243–4258.

Chisham, G., & Pinnock, M. (2002). Assessing the contamination of SuperDARN global convection maps by non-*F*-region backscatter. *Annales Geophysicae*, *20*(1), 13–28. https://doi.org/10.5194/angeo-20-13-2002

Cowley, S. W. H. (1982). The cause of convection in the Earth's magnetosphere: A review of developments during the IMS. *Reviews of Geophysics*, *20*, 531–565. https://doi.org/10.1029/RG020i003p00531

de la Beaujardière, O., Lyons, L. R., & Friis-Christensen, E. (1991). Sondrestrom radar measurements of the reconnection electric field. *Journal of Geophysical Research*, *96*, 13,907–13,912. https://doi.org/10.1029/91JA01174

Dorfman S., Ji, H., Yamada, M., Yoo, J., Lawrence, E., Myers, C., & Tharp, T. (2014). Experimental observation of 3-D, impulsive reconnection events in a laboratory plasma. *Physics of Plasmas 21*(1), 012109. https://doi.org/10.1063/1.4862039

Dorfman, S., Ji, H., Yamada, M., Yoo, J., Lawrence, E., Myers, C., & Tharp, T. D. (2013). Three-dimensional, impulsive magnetic reconnection in a laboratory plasma. *Geophysical Research Letters*, *40*, 233–238. https://doi.org/10.1029/2012GL054574

Fletcher, L., Pollock, J. A., & Potts, H. E. (2004). Tracking of TRACE Ultraviolet Flare Footpoints. *Solar Physics*, *222*, 279.

Goertz, C. K., Nielsen, E., Korth, A., Glassmeier, K. H., Haldoupis, C., Hoeg, P., & Hayward, D. (1985). Observations of a possible ground signature of flux transfer events. *Journal of Geophysical Research*, *90*, 4069–4078. https://doi.org/10.1029/JA090iA05p04069

Greenwald, R. A., Baker, K. B., Dudeney, J. R., Pinnock, M., Jones, T. B., Thomas, E. C., … Yamagishi, H. (1995). DARN/SuperDARN: A global view of the dynamics of high-latitude convection. *Space Science Reviews*, *71*(1-4), 761–796. https://doi.org/10.1007/BF00751350

Haaland, S., Sonnerup, B., Dunlop, M., Balogh, A., Georgescu, E., Hasegawa, H., … Vaivads, A. (2004). Four-spacecraft determination of magnetopause orientation, motion and thickness: Comparison with results from single-spacecraft methods. *Annales Geophysicae*, *22*(4), 1347–1365. https://doi.org/10.5194/angeo-22-1347-2004

Huba, J. D., & Rudakov, L. I. (2002). Three-dimensional Hall magnetic reconnection. *Physics of Plasmas*, *9*(11), 4435–4438. https://doi.org/10.1063/1.1514970

Hubert, B., Milan, S. E., Grocott, A., Blockx, C., Cowley, S. W. H., & Gérard, J.-C. (2006). Dayside and nightside reconnection rates inferred from IMAGE-FUV and Super Dual Auroral Radar Network data. *Journal of Geophysical Research*, *111*, A03217. https://doi.org/10.1029/2005JA011140

Hudson, P. D. (1970). Discontinuities in an anisotropic plasma and their identification in the solar wind. *Planetary and Space Science*, *18*(11), 1611–1622. https://doi.org/10.1016/0032-0633(70)90036-X

Jain, N., Büchner, J., Dorfman, S., Ji, H., & Sharma, A. S. (2013). Current disruption and its spreading in collisionless magnetic reconnection. *Physics of Plasmas 20* (11), 112101. https://doi.org/10.1063/1.4827828

Katz, N., Egedal, J., Fox, W., Le, A., Bonde, J., & Vrublevskis, A. (2010). Laboratory observation of localized onset of magnetic reconnection. *Physical Review Letters*, *104*(25), 255004. https://doi.org/10.1103/PhysRevLett.104.255004

Lapenta, G., Krauss-Varban, D., Karimabadi, H., Huba, J. D., Rudakov, L. I., & Ricci, P. (2006). Kinetic simulations of X-line expansion in 3D reconnection. *Geophysical Research Letters*, *33*, L10102. https://doi.org/10.1029/2005GL025124

Lee, J., & Gary, D. E. (2008). Parallel motions of coronal hard X-ray source and Hα ribbons. *The Astrophysical Journal*, *685*(1), L87–L90. https://doi.org/10.1086/592292

Lee, S. H., Sibeck, D. G., Hwang, K. J., Wang, Y., Silveira, M. V. D., Fok, M. C., … Lester, M. (2016). Inverse energy dispersion of energetic ions observed in the magnetosheath. *Geophysical Research Letters*, *43*, 7338–7347. https://doi.org/10.1002/2016GL069840

Liu, C., Lee, J., Jing, J., Liu, R., Deng, N., & Wang, H. (2010). Motions of hard X-ray sources during an asymmetric eruption. *The Astrophysical Journal*, *721*(2), L193–L198. https://doi.org/10.1088/2041-8205/721/2/L193

McWilliams, K. A., Yeoman, T. K., & Cowley, S. W. H. (2001). Two-dimensional electric field measurements in the ionospheric footprint of a flux transfer event. *Annales Geophysicae*, *18*(12), 1584–1598. https://doi.org/10.1007/s00585-001-1584-2

McWilliams, K. A., Yeoman, T. K., Sibeck, D. G., Milan, S. E., Sofko, G. J., Nagai, T., … Rich, F. J. (2004). Simultaneous observations of magnetopause flux transfer events and of their associated signatures at ionospheric altitudes. *Annales Geophysicae*, *22*(6), 2181–2199. https://doi.org/10.5194/angeo-22-2181-2004

McWilliams, K. A., Yeoman, T. K., Sigwarth, J. B., Frank, L. A., & Brittnacher, M. (2001). The dayside ultraviolet aurora and convection responses to a southward turning of the interplanetary magnetic field. *Annales Geophysicae*, *17*, 707–721.

Milan, S. E., Imber, S. M., Carter, J. A., Walach, M.-T., & Hubert, B. (2016). What controls the local time extent of flux transfer events? *Journal of Geophysical Research: Space Physics*, *121*, 1391–1401. https://doi.org/10.1002/2015JA022012

Milan, S. E., Lester, M., Cowley, S. W. H., & Brittnacher, M. (2000). Convection and auroral response to a southward turning of the IMF: Polar UVI, CUTLASS, and IMAGE signatures of transient magnetic flux transfer at the magnetopause. *Journal of Geophysical Research*, *105*, 15,741–15,755. https://doi.org/10.1029/2000JA900022

Nakamura, T. K. M., Nakamura, R., Alexandrova, A., Kubota, Y., & Nagai, T. (2012). Hall magnetohydrodynamic effects for three-dimensional magnetic reconnection with finite width along the direction of the current. *Journal of Geophysical Research*, *117*, A03220. https://doi.org/10.1029/2011JA017006

Nishimura, Y., Lyons, L. R., Zou, Y., Oksavik, K., Moen, J. I., Clausen, L. B., … Lester, M. (2014). Day-night coupling by a localized flow channel visualized by polar cap patch propagation. *Geophysical Research Letters*, *41*, 3701–3709. https://doi.org/10.1002/2014GL060301

Paschmann, G., Sonnerup, B. U. Ö., Papamastorakis, I., Sckopke, N., Haerendel, G., Bame, S. J., … Elphic, R. C. (1979). Plasma acceleration at the Earth's magnetopause: Evidence for magnetic reconnection. *Nature*, *282*(5736), 243–246. https://doi.org/10.1038/282243a0

Phan, T. D., Paschmann, G., Gosling, J. T., Oieroset, M., Fujimoto, M., Drake, J. F., & Angelopoulos, V. (2013). The dependence of magnetic reconnection on plasma β and magnetic shear: Evidence from magnetopause observations. *Geophysical Research Letters*, *40*, 11–16. https://doi.org/10.1029/2012GL054528

Phan, T. D., Paschmann, G., & Sonnerup, B. U. Ö. (1996). Low-latitude magnetopause and boundary layer for high magnetic shear: 2. Occurrence of magnetic reconnection. *Journal of Geophysical Research*, *101*, 7817–7828. https://doi.org/10.1029/95JA03751

Pinnock, M., Chisham, G., Coleman, I. J., Freeman, M. P., Hairston, M., & Villain, J.-P. (2003). The location and rate of dayside reconnection during an interval of southward interplanetary magnetic field. *Annales Geophysicae*, *21*(7), 1467–1482. https://doi.org/10.5194/angeo-21-1467-2003

Pinnock, M., Rodger, A. S., Baker, K. B., Lu, G., & Hairston, M. (1999). Conjugate observations of the day-side reconnection electric field: A GEM boundary layer campaign. *Annales Geophysicae*, *17*(4), 443–454. https://doi.org/10.1007/s00585-999-0443-4

Pinnock, M., Rodger, A. S., Dudeney, J. R., Baker, K. B., Newell, P. T., Greenwald, R. A., & Greenspan, M. E. (1993). Observations of an enhanced convection channel in the cusp ionosphere. *Journal of Geophysical Research*, *98*, 3767–3776. https://doi.org/10.1029/92JA01382

Provan, G., Yeoman, T. K., & Milan, S. E. (1998). CUTLASS Finland radar observations of the ionospheric signatures of flux transfer events and the resulting plasma flows. *Annales Geophysicae*, *16*(11), 1411–1422. https://doi.org/10.1007/s00585-998-1411-0

Qiu, J. (2009). Observational analysis of magnetic reconnection sequence. *The Astrophysical Journal*, *692*(2), 1110–1124. https://doi.org/10.1088/0004-637X/692/2/1110

Qiu, J., Liu, W., Hill, N., & Kazachenko, M. (2010). Reconnection and energetics in two-ribbon flares: A revisit of the Bastille-Day flare. *The Astrophysical Journal*, *725*(1), 319–330. https://doi.org/10.1088/0004-637X/725/1/319

Qiu, J., Longcope, D. W., Cassak, P. A., & Priest, E. R. (2017). Elongation of flare ribbons. *The Astrophysical Journal*, *838*(1), 17. https://doi.org/10.3847/1538-4357/aa6341

Shay, M. A., Drake, J. F., Swisdak, M., Dorland, W., & Rogers, B. N. (2003). Inherently three dimensional magnetic reconnection: A mechanism for bursty bulk flows? *Geophysical Research Letters*, *30*(6), 1345. https://doi.org/10.1029/2002GL016267

Shepherd, L. S., & Cassak, P. A. (2012). Guide field dependence of 3-D X-line spreading during collisionless magnetic reconnection. *Journal of Geophysical Research*, *117*, A10101. https://doi.org/10.1029/2012JA017867

Sonnerup, B. U., & Cahill, L. J. Jr. (1967). Magnetopause structure and attitude from explorer 12 observations. *Journal of Geophysical Research*, *72*, 171–183. https://doi.org/10.1029/JZ072i001p00171

Southwood, D. J. (1985). Theoretical aspects of the ionospheremagnetosphere-solar wind coupling. *Advances in Space Research*, *5*(4), 7–14. https://doi.org/10.1016/0273-1177(85)90110-3

Trattner, K. J., Mulcock, J. S., Petrinec, S. M., & Fuselier, S. A. (2007). Probing the boundary between antiparallel and component reconnection during southward interplanetary magnetic field conditions. *Journal of Geophysical Research*, *112*, A08210. https://doi.org/10.1029/2007JA012270

Trattner, K. J., Petrinec, S. M., Fuselier, S. A., & Phan, T. D. (2012). The location of reconnection at the magnetopause: Testing the maximum magnetic shear model with THEMIS observations. *Journal of Geophysical Research*, *117*, A01201. https://doi.org/10.1029/2011JA016959

Tsyganenko, N. A. (1995). Modeling the Earth's magnetospheric magnetic field confined within a realistic magnetopause. *Journal of Geophysical Research*, *100*, 5599–5612. https://doi.org/10.1029/94JA03193

Tsyganenko, N. A. (2002a). A model of the magnetosphere with a dawn-dusk asymmetry, 1, mathematical structure. *Journal of Geophysical Research*, *107*(A8), 1179. https://doi.org/10.1029/2001JA000219

Tsyganenko, N. A. (2002b). A model of the near magnetosphere with a dawn-dusk asymmetry, 2. Parameterization and fitting to observations. *Journal of Geophysical Research*, *107*(A8), 1176. https://doi.org/10.1029/2001JA000220

Vasyliunas, V. M. (1984). Steady state aspects of magnetic field line merging. In E. W. Hones, Jr. (Ed.), *Magnetic reconnection in space and laboratory plasmas*, *Geophysical Monograph Series* (Vol. 30, pp. 25–31). Washington, DC: American Geophysical Union.

Walsh, B. M., Komar, C. M., & Pfau-Kempf, Y. (2017). Spacecraft measurements constraining the spatial extent of a magnetopause reconnection X line. *Geophysical Research Letters*, *44*, 3038–3046. https://doi.org/10.1002/2017GL073379

Wang, B., Nishimura, Y., Zou, Y., Lyons, L. R., Angelopoulos, V., Frey, H., & Mende, S. (2016). Investigation of triggering of poleward moving auroral forms using satellite-imager coordinated observations. *Journal of Geophysical Research: Space Physics*, *121*, 10,929–10,941. https://doi.org/10.1002/2016JA023128

Wild, J. A., Cowley, S. W. H., Davies, J. A., Khan, H., Lester, M., Milan, S. E., … Georgescu, E. (2001). First simultaneous observations of flux transfer events at the high-latitude magnetopause by the Cluster spacecraft and pulsed radar features in the conjugate ionosphere by the CUTLASS and EISCAT radars. *Annales Geophysicae*, *19*(10/12), 1491–1508. https://doi.org/10.5194/angeo-19-1491-2001

Wild, J. A., Milan, S. E., Cowley, S. W. H., Dunlop, M. W., Owen, C. J., Bosqued, J. M., … Reme, H. (2003). Coordinated interhemispheric SuperDARN radar observations of the ionospheric response to flux transfer events observed by the Cluster spacecraft at the high-latitude magnetopause. *Annales Geophysicae*, *21*(8), 1807–1826. https://doi.org/10.5194/angeo-21-1807-2003

Zhou, M., Ashour-Abdalla, M., Deng, X., Pang, Y., Fu, H., Walker, R., … Tang, R. (2017). Observation of three-dimensional magnetic reconnection in the terrestrial magnetotail. *Journal of Geophysical Research: Space Physics*, *122*, 9513–9520. https://doi.org/10.1002/2017JA024597

Zou, Y., Nishimura, Y., Burchill, J. K., Knudsen, D. J., Lyons, L. R., Shiokawa, K., … Nishitani, N. (2016). Localized field-aligned currents in the polar cap associated with airglow patches. *Journal of Geophysical Research: Space Physics*, *121*, 10,172–10,189. https://doi.org/10.1002/2016JA022665

Zou, Y., Nishimura, Y., Lyons, L. R., Shiokawa, K., Donovan, E. F., Ruohoniemi, J. M., … Nishitani, N. (2015). Localized polar cap flow enhancement tracing using airglow patches: Statistical properties, IMF dependence, and contribution to polar cap convection. *Journal of Geophysical Research: Space Physics*, *120*, 4064–4078. https://doi.org/10.1002/2014JA020946